Large-area MoS$_2$ grown using H$_2$S as the sulphur source

2D Materials

PAPER

Large-area MoS$_2$ grown using H$_2$S as the sulphur source

Dumitru Dumcenco[1], Dmitry Ovchinnikov[1], Oriol Lopez Sanchez[1], Philippe Gillet[2], Duncan T L Alexander[3], Sorin Lazar[4], Aleksandra Radenovic[5] and Andras Kis[1]

[1] Electrical Engineering Institute, École Polytechnique Fédérale de Lausanne (EPFL), CH-1015 Lausanne, Switzerland
[2] Institute of Condensed Matter Physics, École Polytechnique Fédérale de Lausanne de Lausanne (EPFL), CH-1015 Lausanne, Switzerland
[3] Interdisciplinary Center for Electron Microscopy (CIME), École Polytechnique Fédérale de Lausanne (EPFL), CH-1015 Lausanne, Switzerland
[4] FEI Electron Optics, 5600 KA Eindhoven, The Netherlands
[5] Institute of Bioengineering, École Polytechnique Fédérale de Lausanne (EPFL), CH-1015 Lausanne, Switzerland

E-mail: andras.kis@epfl.ch

Abstract

We report on the growth of molybdenum disulphide (MoS$_2$) using H$_2$S as a gas-phase sulfur precursor that allows controlling the domain growth direction of domains in both vertical (perpendicular to the substrate plane) and horizontal (within the substrate plane), depending on the H$_2$S:H$_2$ ratio in the reaction gas mixture and temperature at which they are introduced during growth. Optical and atomic force microscopy measurements on horizontal MoS$_2$ demonstrate the formation of monolayer triangular-shape domains that merge into a continuous film. Scanning transmission electron microscopy of monolayer MoS$_2$ shows a regular atomic structure with a hexagonal symmetry. Raman and photoluminescence spectra confirm the monolayer thickness of the material. Field-effect transistors fabricated on MoS$_2$ domains that are transferred onto Si/SiO$_2$ substrates show a mobility similar to previously reported exfoliated and chemical vapor deposition-grown materials.

Main text

Molybdenum disulfide (MoS$_2$) has attracted extensive attention for a variety of next generation electrical and optoelectronic device applications because of its unique two-dimensional (2D) nature. In the bulk, this material has a crystalline structure consisting of covalently bonded layers weakly coupled to each other by weak van der Waals forces. Bulk MoS$_2$ is a semiconductor with an indirect bandgap of 1.2 eV [1], whereas monolayer MoS$_2$ shows a direct gap of 1.8 eV [2–4] due to the 2D confinement [5]. Using scotch tape [6] or liquid-phase exfoliation [7, 8] monolayer MoS$_2$ can be easily obtained. Versatile devices including field effect transistors with high on/off current ratio [9], memory cells [10], ultrasensitive photodetectors [11, 12] and nanopores [13] were demonstrated on 2D crystals of MoS$_2$ obtained by mechanical exfoliation from bulk samples.

Nevertheless, exfoliation is not scalable for large-scale device fabrication resulting from the absence of controllable thickness, size and uniformity of the 2D film. Because of this, various chemical synthesis approaches focused on growth of MoS$_2$ have been developed [14–18]. Among them, chemical vapor deposition (CVD) is the most promising method to synthesize monolayer MoS$_2$ from triangular islands up to hundreds of micrometers in size to a large-scale film [17, 18]. Moreover, the proper selection of growth substrate and its pretreatment enables the growth of high-quality centimeter-scale continuous monolayer MoS$_2$ film that is formed from merging single-crystalline domains with the majority of them having the same lattice orientation [19]. In addition to recent reports on monolayer growth, polycrystalline thin films of transition metal dichalcogenides have been prepared by different methods in the past, such as sputtering [20, 21], sulfurization/selenization of transition metal [22–24] or WO$_3$ films [25, 26], sulfurization of thin tungsten films using H$_2$S [27] and sputtering of tungsten in an Ar/H$_2$S atmosphere [28]. Depending on the growth conditions, two types of crystal orientations were obtained, with the basal plane of the crystallites being predominantly oriented either in parallel or perpendicular directions relative to the substrate surface. Recently, a rapid sulfurization/

selenization process to convert Mo and W thin films into polycrystalline molybdenum dichalcogenide films was also demonstrated, where sulfur/selenium powders as the precursors and Ar as a carrier gas were used [29–31]. Due to chemically reactive edge sites, such structures are useful as an active material for catalytic reactions [32, 33].

In addition to the most commonly used CVD methods that involve a solid sulfur source, a highly reactive sulfuric precursor in the form of H_2S has been used for wafer-scale growth of MoS_2 films on different substrates [34–36]. These previously reported growth methods are however unable to produce monolayer MoS_2 due to the relatively large thickness of molybdenum films pre-deposited on insulating substrates and used as the Mo source [34, 35]. Gold-assisted CVD [36], in which an Mo–Au surface alloy is formed during the reaction of $Mo(CO_6)$ with Au thin film, is also unable to produce monolayer MoS_2. Here, we report on the growth of MoS_2 on sapphire substrates using a chemical reaction between MoO_3 and H_2S/H_2 gas mixture as a gas-phase sulfur precursor. Controlling the ratio of $H_2S:H_2$ in the reaction gas mixture and the temperature during growth at which they are injected allow us to regulate the growth direction of domains and switch between multilayer growth in the vertical direction or monolayer growth in the horizontal direction. We find that the injection temperature of the H_2S/H_2 reaction gas mixture is the critical factor for controlling the growth direction, and observe a transition from vertical to horizontal growth modes with decreasing injection temperature. The optical and electrical properties of the horizontal MoS_2 are comparable to those obtained using other growth methods, allowing its use in future electronic and optoelectronic devices.

Growth procedure

Multilayer vertical and monolayer MoS_2 has been grown by CVD on *c*-plane sapphire. Prior to growth, sapphire substrates were consecutively cleaned by acetone/isopropanol/DI-water and then annealed for 1 h at 1000 °C. For growth, they were placed face-down above a crucible containing ~5 mg MoO_3 (⩾99.998% Alfa Aesar) and loaded into a 2 inch split-tube furnace. The temperature is ramped up to 700 °C with a rate of 50 °C min^{-1} and maintained at this target temperature for 10 min, after which the furnace is cooled down to 570 °C with 10 sccm Ar carrier gas flow. The carrier gas flow is then increased to 200 sccm and the furnace opened for rapid cooling. During the growth phase, a mixture of H_2S and H_2 is introduced during the temperature ramp up phase, at different preset-temperatures in the 600 °C–700 °C range. We have tested the effect of different flow rates of the H_2S and H_2 mixture in the 5:15–15:5 sccm range. Flow rates for H_2S and H_2 are maintained constant until the start of the cool-down phase.

TEM and AFM imaging

CVD MoS_2 was transferred from sapphire using the wet transfer KOH method. Samples were first spin coated at 1500 rpm with PMMA A2, resulting in a ~100 nm thick polymer film. These were detached in a 30% KOH solution, washed several times in DI water and transferred onto TEM grids. TEM grids were annealed in a flow of Ar and H_2 for 8 h at 400 °C in order to remove the polymer film. For low-resolution imaging and diffraction studies, 10 nm thick Si_3N_4 windows were used while for high resolution TEM (HR-TEM) we used PELCO Holey Silicon Nitride Support Film with 2.5 um holes in a 200 nm thick Si_3N_4 support. Aberration-corrected scanning transmission electron microscopy (STEM) was performed using a Titan Themis 60-300 (FEI) operated with a beam energy of 80 keV. Medium angle annular dark field imaging conditions were applied with a probe convergence semi-angle of ~28 mrad and a STEM detector collection semi-angle of ~40−200 mrad.
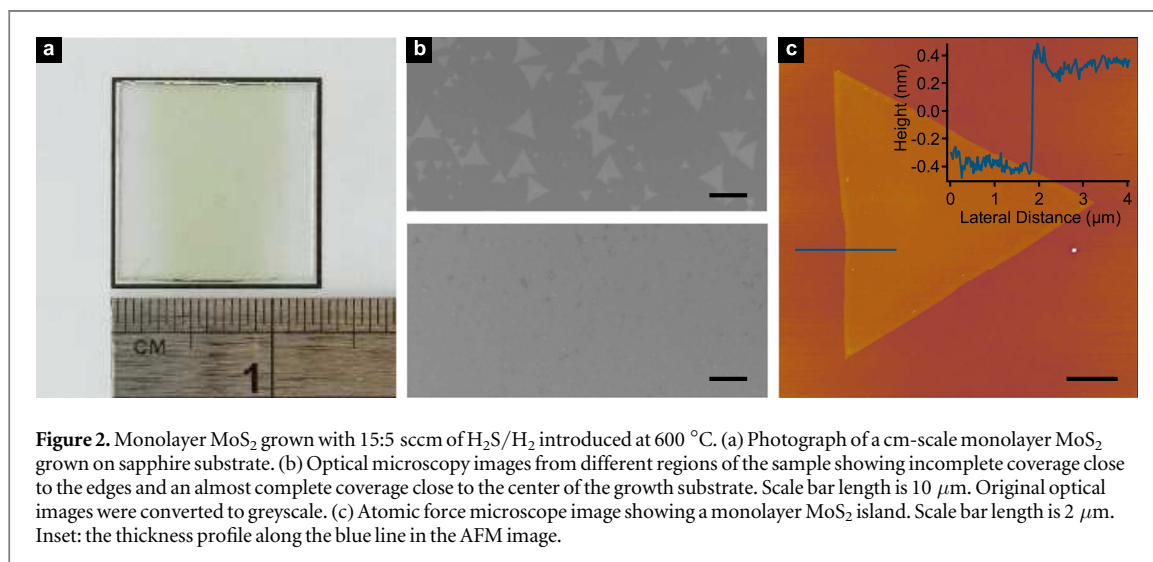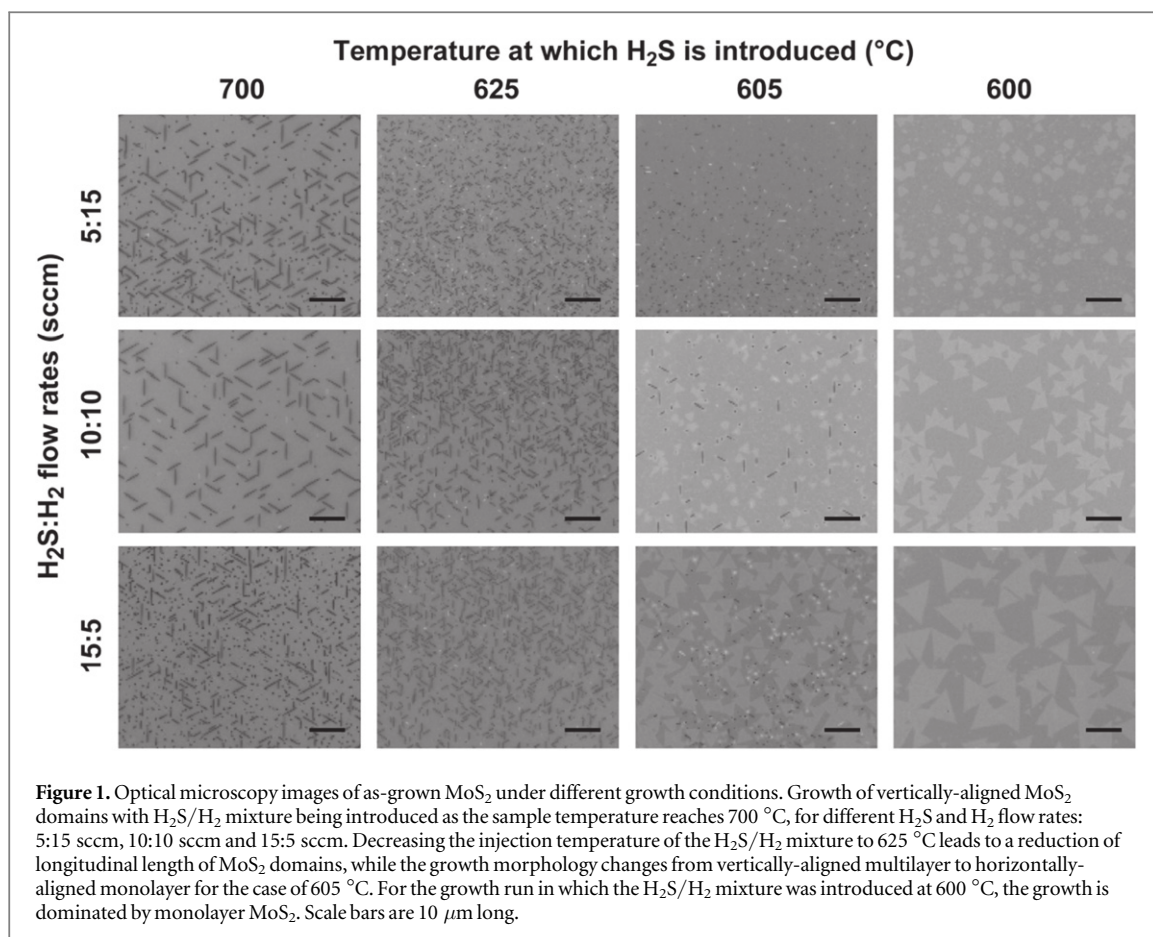
Samples were also imaged using an atomic force microscope (Asylum Research Cypher) operating in AC mode.

Electrical characterization

CVD-grown single domains of MoS_2 were transferred using PMMA A2 as a support film and etching in 30% KOH onto degenerately doped Si substrate covered with 270 nm thick SiO_2. The PMMA film was dissolved in acetone and residues were removed by annealing in Ar atmosphere at 350 °C for 5 h. Electron beam lithography (EBL) was used to define contact regions and 90 nm Au was used as the contact metal. PMMA A4 was used as the etching mask during oxygen plasma etching for some of the devices. The devices were then annealed at 200 °C in Ar atmosphere to eliminate resist residues and reduce contact resistance. Further characterization was performed in vacuum at a base pressure of 10^{-6} mbar after annealing at 140 °C for 24 h.
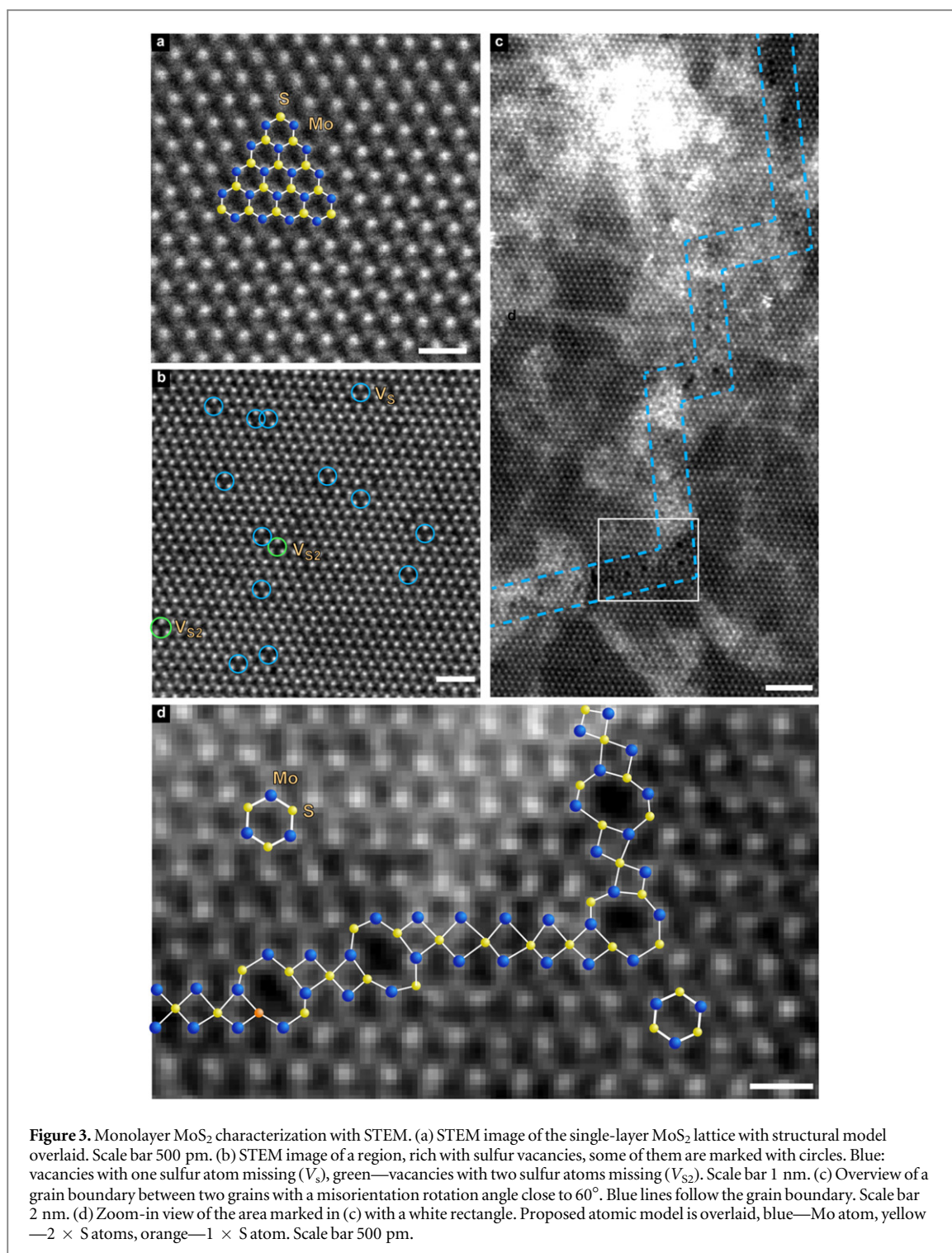
Results

MoS_2 growth using H_2S as a gas-phase sulfur precursor results in highly-oriented vertically-aligned multilayers or horizontally-aligned monolayer domains in the shape of well-defined equilateral triangles (figure 1). At a high H_2S/H_2 injection temperature of 700 °C with different $H_2S:H_2$ ratios (5:15, 10:10 and 15:5 sccm), vertically-aligned multilayer MoS_2 domains with lengths of up to 10 μm have been observed under an optical microscope. The lateral length of MoS_2 domains decreased in size to 4 μm as the temperature at which the H_2S/H_2 mixture is first introduced is lowered to 625 °C. When this temperature is further reduced to 605 °C, together with vertical growth, monolayer MoS_2 domains start to grow in a lateral direction on the surface of the sapphire substrate. For an even lower injection

Figure 1. Optical microscopy images of as-grown MoS$_2$ under different growth conditions. Growth of vertically-aligned MoS$_2$ domains with H$_2$S/H$_2$ mixture being introduced as the sample temperature reaches 700 °C, for different H$_2$S and H$_2$ flow rates: 5:15 sccm, 10:10 sccm and 15:5 sccm. Decreasing the injection temperature of the H$_2$S/H$_2$ mixture to 625 °C leads to a reduction of longitudinal length of MoS$_2$ domains, while the growth morphology changes from vertically-aligned multilayer to horizontally-aligned monolayer for the case of 605 °C. For the growth run in which the H$_2$S/H$_2$ mixture was introduced at 600 °C, the growth is dominated by monolayer MoS$_2$. Scale bars are 10 μm long.

Figure 2. Monolayer MoS$_2$ grown with 15:5 sccm of H$_2$S/H$_2$ introduced at 600 °C. (a) Photograph of a cm-scale monolayer MoS$_2$ grown on sapphire substrate. (b) Optical microscopy images from different regions of the sample showing incomplete coverage close to the edges and an almost complete coverage close to the center of the growth substrate. Scale bar length is 10 μm. Original optical images were converted to greyscale. (c) Atomic force microscope image showing a monolayer MoS$_2$ island. Scale bar length is 2 μm. Inset: the thickness profile along the blue line in the AFM image.

temperature of 600 °C, the growth is dominated by monolayer MoS$_2$ triangles. In general, we observe that an earlier introduction of the H$_2$S/H$_2$ mixture favors horizontal over vertical growth. Moreover, by varying the ratio of the H$_2$S/H$_2$ mixture, the morphology and domain size of monolayer MoS$_2$ flakes is changed. Under more sulphidizing conditions (H$_2$S: H$_2$ = 15:5), optical images reveal that MoS$_2$ domains adopt a triangular shape. This is in accordance with the findings in our previous study with CVD-growth using solid sulfur as a precursor [19], and it suggests

that the triangular shape is the equilibrium form of MoS$_2$ domains under highly sulphurizing conditions. Under reducing (H$_2$S:H$_2$ = 5:15) conditions the triangular domains no longer dominate. Instead, the appearance of another type of MoS$_2$ structure with a hexagonal morphology has been observed. Hence, it appears that the equilibrium shape of MoS$_2$ domains is sensitive to the different gas compositions used in CVD growth. Such domain morphology changes have been observed before for a much higher range of H$_2$S: H$_2$ ratios (500 and 0.07) [37]. Furthermore, according
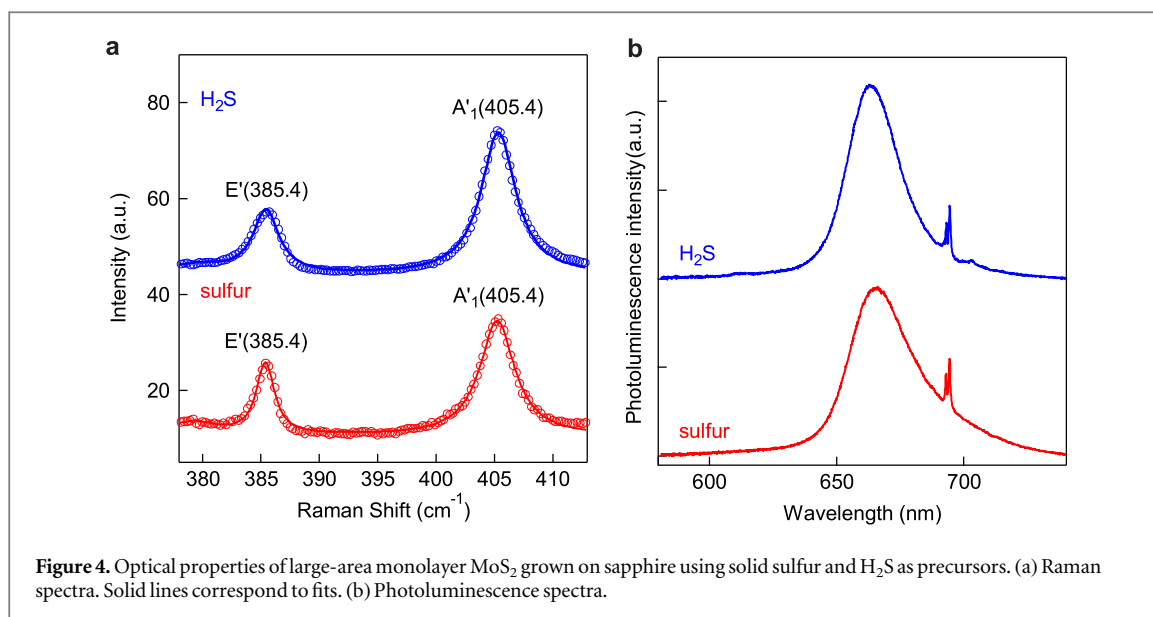
Figure 3. Monolayer MoS_2 characterization with STEM. (a) STEM image of the single-layer MoS_2 lattice with structural model overlaid. Scale bar 500 pm. (b) STEM image of a region, rich with sulfur vacancies, some of them are marked with circles. Blue: vacancies with one sulfur atom missing (V_s), green—vacancies with two sulfur atoms missing (V_{S2}). Scale bar 1 nm. (c) Overview of a grain boundary between two grains with a misorientation rotation angle close to 60°. Blue lines follow the grain boundary. Scale bar 2 nm. (d) Zoom-in view of the area marked in (c) with a white rectangle. Proposed atomic model is overlaid, blue—Mo atom, yellow —2 × S atoms, orange—1 × S atom. Scale bar 500 pm.

to scanning tunneling microscopy results combined with density functional theory calculations, MoS_2 triangles are terminated by dimer-saturated Mo edges, while the hexagonal MoS_2 ones exhibit completely different edge structures with lower sulfur coverage on Mo edges and S edges with adsorbed S–H groups. The presence of H atoms absorbed by S edges means that hexagonal domains could be useful in the hydrodesulfurization process [37].

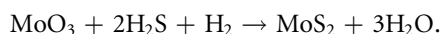We have identified optimal conditions for the growth of single-crystal domains in the shape of well-defined equilateral triangles that merge into a continuous monolayer film, with a 15:5 sccm ratio of H_2S: H_2 gas mixture introduced at 600 °C. It is important to point out that for the syntheses of MoS_2 with solid sulfur as a precursor [19], the sulfurization of MoO_3 is typically performed at 700 °C in an Ar environment, where the chemical reaction is:

$$2MoO_3 + 7S \rightarrow 2MoS_2 + 3SO_2.$$
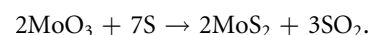
The introduction of the H_2S/H_2 gas mixture as a sulfur precursor in the reaction atmosphere leads to a

Figure 4. Optical properties of large-area monolayer MoS_2 grown on sapphire using solid sulfur and H_2S as precursors. (a) Raman spectra. Solid lines correspond to fits. (b) Photoluminescence spectra.

new, more favorable chemical reaction:

$$MoO_3 + 2H_2S + H_2 \rightarrow MoS_2 + 3H_2O.$$

In this reaction, the H_2S/H_2 ratio in terms of molar volume should be equal to 2.3, which is quite close to the 15:5 ratio of H_2S:H_2 gas mixture obtained for the best growth of monolayer MoS_2. It covers a typical area of 6 mm × 1 cm in the middle portion of the growth substrate using 15:5 ratio of H_2S:H_2 gas mixture injected at 600 °C and followed by a 10 min long growth phase at 700 °C (figure 2(a)). Figures 2(b) and (c) present optical images of different sample regions, showing well separated triangles close to the substrate edge and almost full coverage of MoS_2 film in the substrate center. Figure 2(d) shows an AFM image of an as-grown triangular MoS_2 domain. The AFM line-scan demonstrates the monolayer thickness of single-crystal MoS_2 domains.

TEM characterization
To reveal the atomic structure of the material, we have performed a study of continuous film MoS_2 with aberration-corrected STEM. In order to prevent damage during initial imaging of suspended single layers, in figure 3(a) fast acquisition of several (10–15) frames with 0.5 s per frame has been used. The size of the recorded images was 512 × 512 pixels, which resulted in approximately 2−4 μs per pixel dwell time with a 0.134 Å pixel size. We used beam currents below 50 pA, which resulted in relatively low doses of 3.5×10^4 e Å^{-2}/frame for sub-sequential recording of each frame [38]. Finally, drift-correction and averaging of intensities with Digital Micrograph were used.

Figure 3(a) presents the lattice of MoS_2, imaged in this way and with a negligible beam-induced damage. Here, brighter spots correspond to Mo atoms and darker spots to stacks of two sulfur atoms. In general, contrast in STEM mode under these conditions of monolayer imaging is considered to obey the $Z^{1.7}$

contrast relation [39], which in the absence of contamination allows distinguishing between the atoms with different Z number or between columns with different occupancy. Extracted from Fourier-transformed STEM images and used to draw the overlaid structural model, the lattice constant of $\sim$3.18 Å is in good agreement with the literature values [40]. In the single frame lower magnification images where the dose is even lower (total dose 1.25×10^5 e Å^{-2}) one can see regions with point defects. As illustrated on figure 3(b), we can observe sulfur vacancies with one S atom absent (V_S), while occasionally we also observe vacancies with two missing S atoms (V_{S2}), circled in green. While we cannot completely rule out that these vacancies were introduced during imaging due to beam damage, they could well be inherent to the as-grown material. Indeed, we note that similar point defects were previously observed in CVD MoS_2 [41].

Next we studied the atomic structure of grain boundaries formed by two grains with their relative orientation close to 60°. As shown on figure 3(c), the grain boundary follows a zigzag direction, and is formed mainly by 4- and 8-fold rings.

A mirror twin boundary, which equally corresponds to a 60° relative orientation, has previously been observed to show 20° misorientation zigzag boundary faceting, with a periodic 8-4-4 ring motif along the facets [18]. In our case, although the zigzag misorientation angles are different, 8-fold rings connected by two 4-fold rings are also observed, as shown on figure 3(d). In addition, a chain of five 4-fold rings that connect two differently oriented 8-4-4-8 series of rings was observed. Such a difference is most probably related to the relative translational lattice shift and the small deviation from a perfect 60° orientation between the two grains. Moreover, it has been shown that grain boundaries can consist of distinct 4-fold ring chains forming one-dimensional metallic wires [41].

However, the proposed structure of long 4-fold ring chains would require perfect angle matching and epitaxial growth of MoS_2 on sapphire [19], which was not observed in this case.

Optical properties

The quality of our monolayer MoS_2 has been checked by performing optical characterization. Figure 4(a) shows typical Raman spectra of the CVD material grown on sapphire using H_2S and solid sulfur as precursors [19]. The spectra show two characteristic peaks related to the out-of-plane vibration of S atoms (A_1') with a Raman shift of $\sim 405\,cm^{-1}$ and the in-plane vibration of Mo and S atoms (E') at $\sim 385\,cm^{-1}$. The observed frequency difference confirms that the deposited material is monolayer MoS_2. The position and intensity ratio between the A_1' and E' Raman modes indicate that the quality of both CVD materials is similar.

Figure 4(b) shows typical photoluminescence spectra acquired at room temperature on CVD-grown monolayer MoS_2 grown using H_2S and solid sulfur. From a sample grown by H_2S, we can clearly resolve the intense A excitonic peak positioned at 663 nm (1.87 eV) with a width of ~ 25 nm (~ 70 meV), which is similar to that of the sample grown with sulfur. The B exciton is not expected to be visible at low excitation intensities due to state-filling effects [42]. The sharp doublet at 693 and 694 nm is associated with the presence of Cr^{3+} luminescence centers in the sapphire substrate [43].

Electrical characterization

After characterization of structural and optical properties of our material, we moved to device fabrication and electrical characterization. Material was transferred from sapphire substrates to conventional Si/SiO_2 (270 nm thickness) and contacts were defined by standard EBL. Gold with a thickness of 90 nm was used as the contact material (see methods). Some of the devices were etched in rectangular shape using the second step of EBL followed by oxygen plasma etching.

We characterized our devices in vacuum (base pressure 10^{-6} mbar) after annealing at $140\,°C$ for 24 h. We present the characteristics of a typical device after annealing on figure 5. This device was etched in rectangular shape. I_s–V_g characteristic is shown on figure 5(a), with $V_s = 1$ V applied. The field-effect mobility, extracted from two-contact measurements is presented on figure 5(b). We used the following expression to extract two-probe mobility: $\mu_{2C} = [L/W] \times \left[dG_{2C}/dV_g \right] \times [1/C_{ox}]$, where G_{2C} stands for two-probe conductivity, $C_{ox} = 1.28 \times 10^{-8}\,F\,cm^{-2}$—geometrical capacitance of 270 nm thick SiO_2, normalized per unit area. The two-probe mobility, which does not take into account the effect of contact resistance, presents the lower estimate of
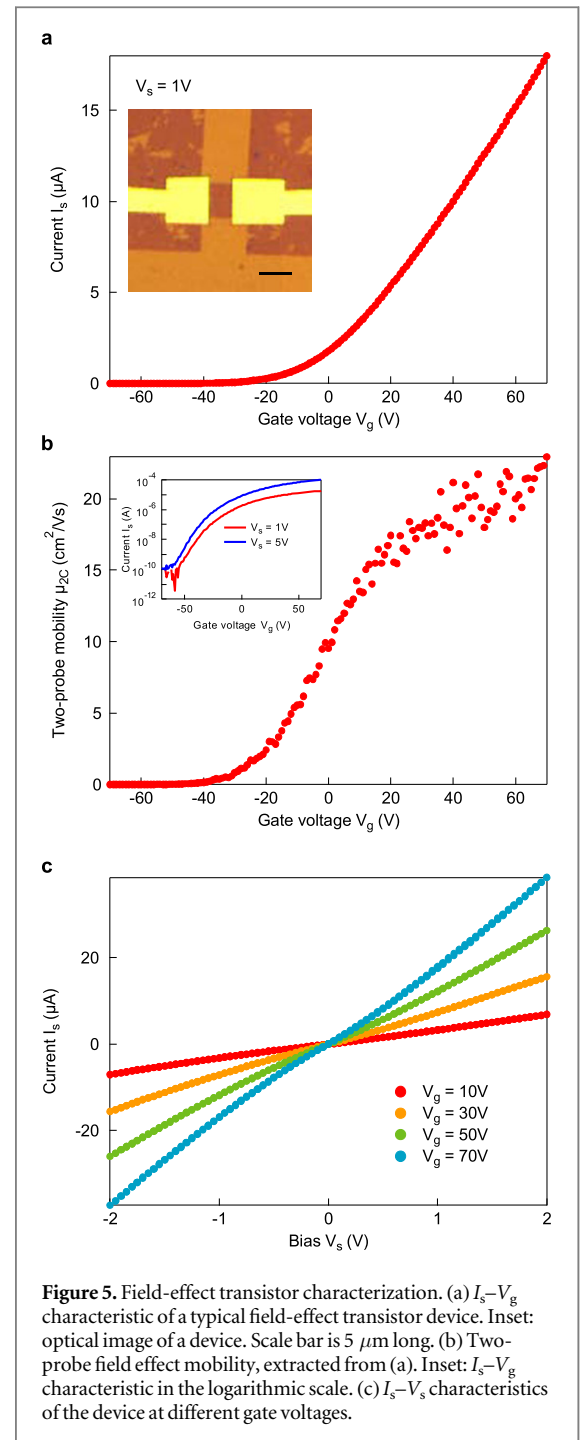

Figure 5. Field-effect transistor characterization. (a) I_s–V_g characteristic of a typical field-effect transistor device. Inset: optical image of a device. Scale bar is 5 μm long. (b) Two-probe field effect mobility, extracted from (a). Inset: I_s–V_g characteristic in the logarithmic scale. (c) I_s–V_s characteristics of the device at different gate voltages.

intrinsic properties of the material. Values of $\mu_{2C} \sim 20\,cm^2\,V^{-1}\,s^{-1}$ are in good agreement with recent reports on CVD MoS_2, grown from solid precursors on SiO_2 [44] and sapphire [19] substrates, which indicates a similar quality of material. We estimate an I_{on}/I_{off} ratio $\sim 10^6$ of this transistor at $V_s = 5$ V from the blue curve in the inset of figure 5(b). Finally, we inspect the quality of injection, performing I_s–V_s sweeps with the fixed gate voltages, shown on figure 5(c).

Overall, the device characteristics demonstrate good current injection and mobility, high I_{on}/I_{off} ratio and electron doping of the channel, typical for exfoliated or CVD material. The observed doping levels are most probably related to sulfur vacancies and other

clusters of defects, as observed in our material by STEM.

Conclusion

In conclusion, we have demonstrated controlling growth direction of MoS_2 domains by CVD using H_2S as a gas-phase precursor instead of conventional sulfur. Optical and electrical measurements on material grown in the horizontal direction, i.e. in-plane of the substrate, demonstrated the high quality of our samples, similar to previous results on exfoliated and CVD-grown samples. Aside from in-plane monolayer MoS_2, the proposed growth strategy involving the replacement of solid sulfur by H_2S gas precursor also permits one to obtain vertically grown multilayer structures that may have various electrochemical applications due to chemically reactive edge sites.

Acknowledgments

References

[1] Kam K and Parkinson B 1982 *J. Phys. Chem.* **86** 463
[2] Lebègue S and Eriksson O 2009 *Phys. Rev. B* **79** 115409
[3] Splendiani A, Sun L, Zhang Y, Li T, Kim J, Chim C-Y, Galli G and Wang F 2010 *Nano Lett.* **10** 1271
[4] Mak K, Lee C, Hone J, Shan J and Heinz T 2010 *Phys. Rev. Lett.* **105** 2
[5] Kuc A, Zibouche N and Heine T 2011 *Phys. Rev. B* **83** 245213
[6] Novoselov K S, Jiang D, Schedin F, Booth T J, Khotkevich V V, Morozov S V and Geim A K 2005 *Proc. Natl Acad. Sci. USA* **102** 10451
[7] Coleman J N *et al* 2011 *Science* **331** 568
[8] Smith R J *et al* 2011 *Adv. Mater.* **23** 3944
[9] Radisavljevic B, Radenovic A, Brivio J, Giacometti V and Kis A 2011 *Nat. Nanotechnology* **6** 147
[10] Bertolazzi S, Krasnozhon D and Kis A 2013 *ACS Nano* **8** 3246
[11] Lopez-Sanchez O, Lembke D, Kayci M, Radenovic A and Kis A 2013 *Nat. Nanotechnology* **8** 497
[12] Yin Z, Li H, Li H, Jiang L, Shi Y, Sun Y, Lu G, Zhang Q, Chen X and Zhang H 2012 *ACS Nano* **6** 74
[13] Liu K, Feng J, Kis A and Radenovic A 2014 *ACS Nano* **8** 2504
[14] Liu K-K *et al* 2012 *Nano Lett.* **12** 1538
[15] Zhan Y, Liu Z, Najmaei S, Ajayan P M and Lou J 2012 *Small* **8** 966
[16] Lee Y-H *et al* 2012 *Adv. Mater.* **24** 2320
[17] Najmaei S, Liu Z, Zhou W, Zou X, Shi G, Lei S, Yakobson B I, Idrobo J-C, Ajayan P M and Lou J 2013 *Nat. Mater.* **12** 754
[18] van der Zande A M, Huang P Y, Chenet D A, Berkelbach T C, You Y, Lee G-H, Heinz T F, Reichman D R, Muller D A and Hone J C 2013 *Nat. Mater.* **12** 554
[19] Dumcenco D *et al* 2015 *ACS Nano* **9** 4611
[20] Stewart T B and Fleischauer P D 1982 *Inorg. Chem.* **21** 2426
[21] Bichsel R and Levy F 1984 *Thin Solid Films* **116** 367
[22] Jäger-Waldau A, Lux-Steiner M, Jäger-Waldau R, Burkhardt R and Bucher E 1990 *Thin Solid Films* **189** 339
[23] Jäger-Waldau A and Bucher E 1991 *Thin Solid Films* **200** 157
[24] Jäger-Waldau A, Lux-Steiner M C, Bucher E, Scandella L, Schumacher A and Prins R 1993 *Appl. Surf. Sci.* **65–66** 465
[25] Galun E, Cohen H, Margulis L, Vilan A, Tsirlina T, Hodes G, Tenne R, Hershfinkel M, Jaegermann W and Ellmer K 1995 *Appl. Phys. Lett.* **67** 3474
[26] Matthäus A, Ennaoui A, Fiechter S, Tiefenbacher S, Kiesewetter T, Diesner K, Sieber I, Jaegermann W, Tsirlina T and Tenne R 1997 *J. Electrochem. Soc.* **144** 1013
[27] Genut M, Margulis L, Hodes G and Tenne R 1992 *Thin Solid Films* **217** 91
[28] Ellmer K, Stock C, Diesner K and Sieber I 1997 *J. Cryst. Growth* **182** 389
[29] Kong D, Wang H, Cha J J, Pasta M, Koski K J, Yao J and Cui Y 2013 *Nano Lett.* **13** 1341
[30] Gaur A P S, Sahoo S, Ahmadi M, Guinel M J-F, Gupta S K, Pandey R, Dey S K and Katiyar R S 2013 *J. Phys. Chem. C* **117** 26262
[31] Jung Y, Shen J, Liu Y, Woods J M, Sun Y and Cha J J 2014 *Nano Lett.* **14** 6842
[32] Hinnemann B, Moses P G, Bonde J, Jørgensen K P, Nielsen J H, Horch S, Chorkendorff I and Nørskov J K 2005 *J. Am. Chem. Soc.* **127** 5308
[33] Jaramillo T F, Jørgensen K P, Bonde J, Nielsen J H, Horch S and Chorkendorff I 2007 *Science* **317** 100
[34] Lee Y, Lee J, Bark H, Oh I-K, Ryu G H, Lee Z, Kim H, Cho J H, Ahn J-H and Lee C 2014 *Nanoscale* **6** 2821
[35] Wang J, Chen L, Lu W, Zeng M, Tan L, Ren F, Jiang C and Fu L 2014 *RSC Adv.* **5** 4364
[36] Song I, Park C, Hong M, Baik J, Shin H-J and Choi H C 2014 *Angew. Chem., Int. Ed Engl.* **53** 1266
[37] Lauritsen J V, Bollinger M V, Lægsgaard E, Jacobsen K W, Nørskov J K, Clausen B S, Topsøe H and Besenbacher F 2004 *J. Catal.* **221** 510
[38] Zan R, Ramasse Q M, Jalil R, Georgiou T, Bangert U and Novoselov K S 2013 *ACS Nano* **7** 10167
[39] Krivanek O L *et al* 2010 *Nature* **464** 571
[40] Brivio J, Alexander D T L and Kis A 2011 *Nano Lett.* **11** 5148
[41] Zhou W, Zou X, Najmaei S, Liu Z, Shi Y, Kong J, Lou J, Ajayan P M, Yakobson B I and Idrobo J-C 2013 *Nano Lett.* **13** 2615
[42] Plechinger G, Mann J, Preciado E, Barroso D, Nguyen A, Eroms J, Schüller C, Bartels L and Korn T 2014 *Semicond. Sci. Technol.* **29** 064008
[43] Kudryashov V E, Mamakin S S and Yunovich A É 1999 *Tech. Phys. Lett.* **25** 536
[44] Schmidt H *et al* 2014 *Nano Lett.* **14** 1909